Modelling magnetic exchange springs in 1D, 2D, and 3D

2008 J. Phys.: Condens. Matter 20 015209

(http://iopscience.iop.org/0953-8984/20/1/015209)

J. Phys.: Condens. Matter **20** (2008) 015209 (8pp) doi:10.1088/0953-8984/20/01/015209

Modelling magnetic exchange springs in 1D, 2D, and 3D

G J Bowden[1], **K N Martin, B D Rainford and P A J de Groot**

School of Physics and Astronomy, University of Southampton, SO17 1BJ, UK

E-mail: gjb@phys.soton.ac.uk

Received 9 July 2007, in final form 5 November 2007
Published 29 November 2007
Online at stacks.iop.org/JPhysCM/20/015209

Abstract

1D models of magnetic multilayers, with alternating hard and soft layers, are extended to 2D and 3D, and presented within a common framework of nearest neighbour interactions. Using 2D calculations, it is shown that the properties of magnetic exchange springs can be changed significantly by patterning the hard pinning layers. But, in certain cases the bending field B_B is not significantly altered, even when half the pinning layer is removed. 3D calculations are used to probe the effects of defects on the properties of magnetic exchange springs, using epitaxial $DyFe_2/YFe_2$ superlattices as an example. It is shown that point defects such as Fe vacancies have little effect on the bending field transition. This is in marked contrast to the 1D model, where an Fe vacancy cuts the magnetic exchange spring into two. Finally, it is demonstrated that significant changes in the properties of magnetic exchange springs can be engineered, by placing rare-earth ions in the centre of the soft YFe_2 springs. A new phenomenon, *exchange spring collapse*, is predicted.

(Some figures in this article are in colour only in the electronic version)

1. Introduction

In recent years, the properties of magnetic exchange springs have attracted much attention. For example, Fullerton *et al* (1998, 1999), Jiang *et al* (2004) have studied the bi-layer system $SmCo_5/Fe$. Here, the hard $SmCo_5$ layer pins one side of the magnetically soft Fe layer. On the other hand, Sawicki *et al* (2000), Dumesnil *et al* (2000), Zimmermann *et al* (2006), Fitzsimmons *et al* (2006) have worked on epitaxially grown $REFe_2/YFe_2$ superlattices. Here it is the YFe_2 which forms the soft layer. One of the early reasons for this work stemmed from the papers of Kneller (1991), Coey and Skomski (1993), who argued, on theoretical grounds, that composite magnets with a giant energy product $(BH)_{MAX}$ of 120 MGOe might be feasible. However recently, other features such as exchange spring assisted data storage schemes have been proposed (Ulrich *et al* 2004). In addition, the discovery of giant magneto-resistance, driven by exchange springs (Gordeev *et al* 2001), opens up potential applications in device sensors.

From the theoretical point of view, a key paper, detailing the magnetic behaviour of a hard magnetic substrate coated with a soft Fe layer, was first given by Goto *et al* (1965). These authors showed that the angular dependence of a planar exchange spring in a bi-layer sample, could be expressed in terms of Jacobi elliptic functions. They showed, both theoretically and experimentally, that the onset of the exchange spring was characterized by a critical bending field B_B which was proportional to $1/d^2$, where d is the thickness of the soft magnetic layer. This work has been extended by Bowden *et al* (2000) to discrete bi-layer and multilayer exchange springs. In particular, it was shown that the bending field transition B_B is related to the Fe–Fe exchange field B_{EX} by the simple relationship $B_B = B_{EX}(\pi/N)^2$ (multilayer) and $B_B = B_{EX}(\pi/2N)^2$ (bi-layer), where the soft layers are pinned at the hard interfaces and N is the number of monolayers in the magnetically soft layer,. Finally, it should be noted in addition to the first order requirement $\partial E_{tot}/\partial\theta_i = 0$ for all $\{\theta_i\}$, it is also necessary to ensure that the $N \times N$ second order matrix $\mathbf{E}_0'' = \{\partial^2 E_{tot}/\partial\theta_i\partial\theta_j\}$ (for planar spins) is positive semi-definite. For example, if $\mathbf{E}_0''$ possesses one negative root, the spin-arrangement $\{\theta_i\}$ is unstable (Bowden *et al* 2003).

In this paper, the 1D work of Goto *et al*, and other authors is extended to two and three dimensions. The paper is set out as follows. In sections 2 and 3, a common framework for 1D, 2D and 3D models is adopted, based on a nearest neighbour interaction model. It is shown that for simple planar

[1] Author to whom any correspondence should be addressed.

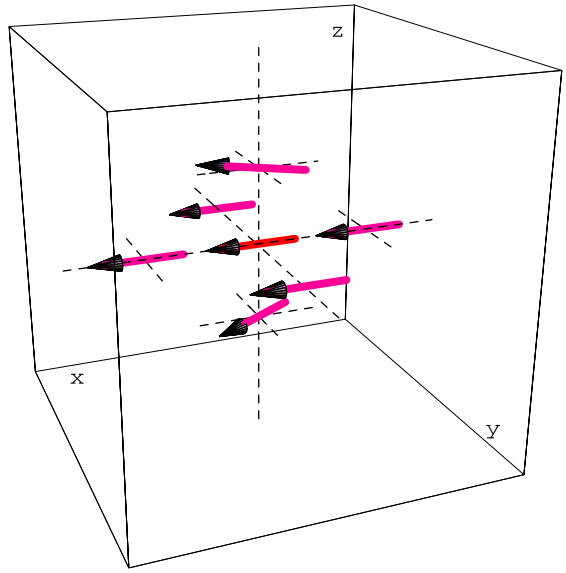

Figure 1. A small section of a planar exchange spring directed along the z-axis. The centre ion is surrounded by four parallel interacting neighbours in the x–y plane, while the moments above and below the centre ion are twisted with respect to each other.

springs, all models predict the same bending field B_B. In section 4, 2D calculations are presented which demonstrate that the properties of domain walls can be significantly altered by modifying the hard pinning layers. Finally, in sections 5 and 6, 3D results are presented which probe the effects of defects on the properties of magnetic exchange springs in the $DyFe_2/YFe_2$ system. It is shown that singular point defects such as Fe vacancies have little effect on the bending field transition, in marked contrast to the 1D model, where a single Fe vacancy simply cuts a magnetic exchange spring into two. However when RE ions are placed in the middle of the soft YFe_2 springs, significant changes can be brought about.

2. 1D, 2D and 3D models of a magnetic exchange spring

In this section, we cast the 1D, 2D and 3D models of a magnetic exchange spring into a common framework. For simplicity, we assume that the exchange spring is a simple planar type with the screw-axis directed along the z-direction i.e. perpendicular to the plane of the multilayer. It will be shown that the bending fields and energies are all the same, regardless of dimension.

For convenience, we start with the 3D model shown schematically in figure 1. Here, we show a small portion of a magnetic exchange springing in elemental iron. Note that the Fe moments are assumed to sit on a cubic lattice, with nearest neighbour interactions only. Moreover, the moments, in any given monolayer perpendicular to the z-axis, are all aligned parallel to each other.

The energy of such a spring can be written in the form:

$$E_{\rm tot} = \sum_{i}^{N}\sum_{j}^{N}\sum_{k}^{N}\varepsilon_{i,j,k} \tag{1}$$

where $\varepsilon_{i,j,k}$, the energy of the centre-ion, is given by:

$$\begin{aligned}\varepsilon_{i,j,k} = &-\tfrac{1}{6}\mu_{\rm FE}B_{\rm EX}\big[\cos(\theta_{i,j,k+1}-\theta_{i,j,k})\\ &+\cos(\theta_{i,j,k}-\theta_{i,j,k-1})\big]-\tfrac{2}{3}\mu_{\rm FE}B_{\rm EX}\\ &-K_A(i)\cos^2\theta_{i,j,k}-\mu(i)B_{\rm APP}\cos\left(\theta_{i,j,k}-\theta_H\right).\end{aligned} \tag{2}$$

Here, (i) $B_{\rm EX}$ and $B_{\rm APP}$ are the magnetic exchange and applied fields, respectively, (ii) the magnetic field is applied in the plane along θ_H, and (iii) $K_{\rm A}$ is a simple axial in-plane anisotropy, which is usually set equal to zero in the soft layers. Note the appearance of the $-\frac{2}{3}\mu_{\rm FE}B_{\rm EX}$ term in equation (2). This represents the exchange energy arising from the four parallel and co-planar spins in the x–y plane.

Next we observe that the 1D model can be expressed in almost identical form:

$$E_{\rm tot} = \sum_{k=1}^{N}\varepsilon_k \tag{3}$$

where

$$\begin{aligned}\varepsilon_k = &-\tfrac{1}{6}\mu_{\rm FE}B_{\rm EX}\left[\cos(\theta_{k+1}-\theta_k)+\cos(\theta_k-\theta_{k-1})\right]\\ &-\tfrac{2}{3}\mu_{\rm FE}B_{\rm EX}-K_{\rm A}(i)\cos^2\theta_k-\mu(i)\\ &\times B_{\rm APP}\cos\left(\theta_k-\theta_H\right).\end{aligned} \tag{4}$$

Note that this expression differs from that of Goto *et al* (1965), Fullerton *et al* (1998, 1999), Fitzsimmons *et al* (2006) and others, in two respects. Firstly, Goto *et al* assume that the exchange energy is generated by neighbouring $k\pm1$ layers, on the kth ion. Secondly, there is an extra exchange term $-\frac{2}{3}\mu_{\rm FE}B_{\rm EX}$ in equation (4), arising from the four in-plane parallel 'ghost-spins'. Note that if all the spins are parallel, the full single-ion exchange term $-\mu_{\rm FE}B_{\rm EX}$ is recovered.

With this proviso it is easy to see that the energy per ion, in both the ferromagnetic and planar–spiral states, in both the 1D and 3D models under consideration, are identical. Thus the bending fields, magnetic loops etc, are the same. A similar argument can also be mounted for the 2D model, again for the case of a simple planar spiral. However in this case, the amount of energy contributed by two ghost spins is $-\frac{1}{3}\mu_{\rm FE}B_{\rm EX}$. In practice, this common framework confers great advantages. For example, it is often possible to check say a 3D result with a faster 1D calculation.

However, the existence of more complicated spiral states, involving angular dispersion in more than two dimensions, is possible. In such cases, the use of a 1D model is inappropriate. In such cases, it is mandatory to use either the general 2D or 3D model. For 2D:

$$\begin{aligned}\varepsilon_{i,j} = N\big\{&-\mu_{\rm FE}B_{\rm EX}\tfrac{1}{6}\big[\cos(\theta_{i+1,j}-\theta_{i,j})+\cos(\theta_{i,j}-\theta_{i-1,j})\\ &+\cos(\theta_{i,j+1}-\theta_{i,j})+\cos(\theta_{i,j}-\theta_{i,j-1})\big]\\ &-\tfrac{1}{3}\mu_{\rm FE}B_{\rm EX}-K_A(i)\cos^2\theta_{i,j}\\ &-\mu(i)B_{\rm APP}\cos\left(\theta_{i,j}-\theta_H\right)\big\}\end{aligned} \tag{5}$$

while in 3D:

$$\begin{aligned}\varepsilon_{i,j,k} = &-\mu_{\rm FE}B_{\rm EX}\tfrac{1}{6}[\cos(\theta_{i+1,j,k}-\theta_{i,j,k})\\ &+\cos(\theta_{i,j,k}-\theta_{i-1,j,k})+\cos(\theta_{i,j+1,k}-\theta_{i,j,k})\\ &+\cos(\theta_{i,j,k}-\theta_{i,j-1,k})+\cos(\theta_{i,j,k+1}-\theta_{i,j,k})\\ &+\cos(\theta_{i,j,k}-\theta_{i,j,k-1})]-K_A(i)\cos^2\theta_{i,j,k}\\ &-\mu(i)B_{\rm APP}\cos\left(\theta_{i,j,k}-\theta_H\right).\end{aligned} \tag{6}$$

Of course, in general, it is best to use the full 3D model with generalized angles $\{\theta_{i,j,k}, \phi_{i,j,k}\}$. Such a model will converge ultimately to an appropriate exchange spring state, planar or otherwise. However there are many cases where to reduce computing time, the use of lower dimensional models is mandatory. In this regard, it is also worth noting that the time required to find the shape of the exchange spring in a repetitive multilayer film can be reduced significantly, using cyclic boundary conditions. For example, in the 1D model we set:

$$\theta_0 = \theta_N; \qquad \theta_{N+1} = \theta_1 \tag{7}$$

where N is the number of monolayers in each bi-layer.

Finally, for stability, the partial derivative of the total energy, with respect to small variations in θ_i, must be zero. In the 1D model therefore:

$$\frac{\partial E_{\text{tot}}}{\partial \theta_k} = N^2\{-\mu_{\text{Fe}} B_{\text{EX}} \{\sin(\theta_{k+1} - \theta_k) - \sin(\theta_k - \theta_{k-1})\} + K_A(k) \sin 2\theta_k + \mu(k) B_{\text{APP}} \sin(\theta_k - \theta_H)\} = 0. \tag{8}$$

In practice, this equation is sufficient to define the shape of the magnetic exchange spring. This is usually done using numerical methods and there is extensive literature on this problem. The reader is referred to (i) the iterative procedure of Trallori *et al* (1994, 1996), and Amato *et al* (1999, 2000), (ii) the Monte Carlo method of Fullerton *et al* (1998, 1999), and (iii) the linearized procedure of Bowden *et al* (2000, 2003). In this paper, we use the latter because this method readily lends itself to a discussion of stability. But, while equation (8) can be used to define the shape of an exchange spring, it cannot be used to decide whether the solution represents a minimum or maximum in the energy E_{tot}. This point can be settled by an examination of the eigenvalues of the double energy derivative $N \times N$ matrix $\mathbf{E}_0''$, where N is the number of independent variables. If the lowest energy eigenvalue is positive semi-definite, for a given set of angles $\{\theta_i\}$, the solution represents a minimum in the energy surface E_{tot}. In addition, it is also worth noting that more information can be gained by examining the eigenvectors of the lowest eigenvalues of $\mathbf{E}_0''$. For example, as the magnetic field approaches the bending field transition B_{B}, the eigenstate just above the AF ground state reveals the incipient presence of a magnetic exchange spring.

3. Estimates of the Fe–Fe exchange field B_{EX}

In this section, we review the estimates of the Fe–Fe exchange field B_{EX} used by several authors in their discussion of magnetic exchange spring systems. In addition, we define a simple cubic 3D model which is used to represent the anti-ferromagnetic cubic Laves $REFe_2$ compounds.

Following Fullerton *et al* (1998, 1999) the exchange field at the kth site in a 1D model takes the form:

$$\varepsilon_k(\text{EX}) = -\frac{A}{d^2}\left[\cos(\theta_{k+1} - \theta_k) + \cos(\theta_k - \theta_{k-1})\right]. \tag{9}$$

Thus:

$$\mu_{\text{Fe}} B_{\text{EX}} = \frac{2A}{d^2}. \tag{10}$$

For soft iron layers Fullerton *et al* (1998) give $A \approx 2.8 \times 10^{-6}$ ergs cm^{-1} and $d = 2$ Å. On using $n_{\text{Fe}} = 8.47 \times 10^{22}$ Fe atoms cm^{-3}, we find $\mu_{\text{Fe}} B_{\text{EX}} = 1191$ K per iron moment. This is in accord with general expectations, since the Curie temperature for Fe is 1070 K, and we expect $\mu_{\text{Fe}} B_{\text{EX}} \sim T_{\text{C}}$. We turn now to a discussion of the $REFe_2$ Laves phase compounds.

First, we note that the magnetic hysteresis curves of several $DyFe_2/YFe_2$ superlattices have already been well modelled at low temperatures (10 K) using a simple planar 1D spring model with the parameters $K_{\text{A}}(\text{Dy}) \sim 10$ K ([001] easy axis), $K_{\text{A}}(\text{Y}) = 0$, $B_{\text{EX}} = 600$ T, $M_{\text{YFe}_2} = 3.0\ \mu_{\text{B}}$, $M_{\text{DyFe}_2} = 7.0\ \mu_{\text{B}}$ (i.e. $\mu_{\text{Fe}} = 1.5\ \mu_{\text{B}}$ and $\mu_{\text{Dy}} = 10\ \mu_{\text{B}}$) and setting one monolayer of the $DyFe_2$ equal to 2.5Å (Bowden *et al* 2003). For the purposes of comparison therefore, these are the values used in this paper, except for the revised estimates of Fe–Fe exchange field B_{EX} and monolayer spacing d discussed below. In passing, we note that there is a small magnetic moment $\approx -0.4\ \mu_{\text{B}}$ on the Y sites (Armitage *et al* 1989). For present purposes however, we chose to ignore the small Y moment, given the errors in estimates of rather more important parameters.

Fitzsimmons *et al* (2006) have given estimates of A for Fe–Fe exchange field in YFe_2 and $DyFe_2$. These were derived from neutron-reflectrometry data, fitted to a 1D planar exchange spring model. Using their quoted figures we find $\mu_{\text{Fe}} B_{\text{EX}} = 24\,803(3011)$ K for $YFe_2(DyFe_2)$, respectively. Since the Curie temperatures of these two compounds are ~600 K, we must conclude that these estimates are too high. Moreover, given that the Curie temperature of these two compounds are similar (542 K for YFe_2 and 635 K for $DyFe_2$, Buschow 1977), it would appear that there is little reason for the difference (~8) in the quoted Fe–Fe exchange fields for these two compounds. In general, we expect $\mu_{\text{FE}} B_{\text{EX}} \approx 600$ K for the $REFe_2$ compounds, but we would like to do better.

In practice, the exchange field we adopt depends on the spacing d between the Fe–Fe layers. For the $REFe_2$ compounds, the choice of d is non-trivial. The spacing between the Fe–Fe layers, and their relative populations, are direction dependent. For a magnetic exchange springs, in different directions, this poses a problem. We choose instead to set up the simple cubic representation of the cubic Laves $DyFe_2$ compound shown in figure 2. Here the volume associated with each $DyFe_2$ formula unit has been set at $(a/2)^3$, where the cubic lattice constant $a = 7.325$ Å for $DyFe_2$ (Buschow 1977). Note that from the micro-magnetic modelling point of view, the magnetization $m = (\mu_{\text{Dy}} - 2\mu_{\text{Fe}})$ per unit cell $(a/2)^3$ is faithfully reproduced. Thus we set $d = 3.66$ Å. Finally, for simplicity we have assumed that the anti-ferromagnetic exchange between the RE and Fe moments is infinite. This is not strictly true, but if we allow non-co-linearity this will double the number of variables $\{\theta_i, \phi_i\}_{\text{Fe}} \rightarrow \{\theta_i, \phi_i\}_{\text{Fe}} + \{\theta_i, \phi_i\}_{\text{RE}}$.

Having made a choice for the spacing d, we now need to obtain an estimate for the exchange field. As mentioned earlier, Bowden *et al* (2000) have given a very simple formula for infinitely pinned exchange springs (see section 1). However, in the 3D model, and revised 1D model, only 1/3 of the exchange

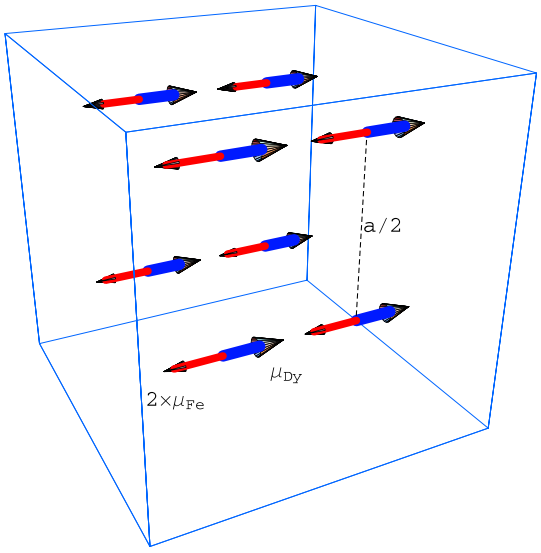

Figure 2. Simple cubic representation of the Laves $REFe_2$ compound. At each site the magnetic moment $m = (\mu_{Dy} - 2\mu_{Fe})$. The spacing between the sites is $a/2$.

field is involved in the creation of a planar exchange spring. We write therefore:

$$B_B = \frac{1}{3}B_{EX}\left(\frac{\pi}{N}\right)^2 \qquad \text{(multilayer)}$$
$$B_B = \frac{1}{3}B_{EX}\left(\frac{\pi}{2N}\right)^2 \qquad \text{(bilayer)}. \tag{11}$$

Note the intimate connection between the exchange field B_{EX} and N the number of monolayers, which in turn involves the monolayer spacing d.

Given equation (11) we can now obtain an estimate for B_{EX}, using the experimentally determined bending fields B_B for various $DyFe_2/YFe_2$ multilayers (Sawicki *et al* 2000). On fitting their data to the formula: $B_B = k/t^m$ (multilayer), where t is the thickness of YFe_2 layers, the aforementioned authors found $m = 1.83(12)$ and $\text{Log}[k] = 4.1(2)$. Since one of their primary aims was to show that the exponent $m \sim 2$, we have chosen to re-analyse their results by setting the exponent $m = 2$. We find $k = 4.40(03)$, which can be used to extract a value of B_{EX} of 570(45) (T), for a d of 3.66 Å. In passing, we should note that equation (11) only holds for infinitely pinned exchange springs. However calculations, particularly at low temperatures, reveal that the bending field is determined primarily by the interplay between the exchange and applied magnetic fields. So our estimate of B_{EX} of 570(45) (T) for $d = 3.66$ Å, probably represents the best that one can do at the present time. Note that for a Fe-moment of 1.5 μ_B, $\mu_{Fe}B_{EX} \approx 572$ K, close to the Curie temperatures of these compounds.

4. Patterned walls in 2D magnetic exchange springs

An example of a 2D calculation for a nominal $DyFe_2/YFe_2$ multilayer can be seen in figure 3. Note that (i) when cyclic

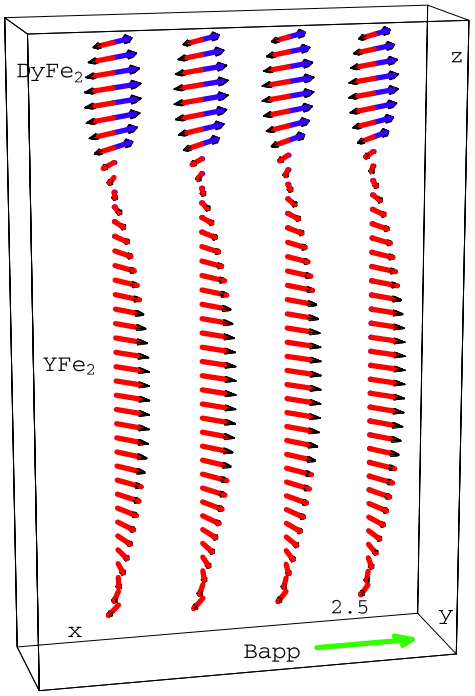

Figure 3. A 2D exchange spring for four strings with $N_x = 4$ and $N_z = (32)_{YFe_2} + (8)_{DyFe_2}$, and cyclic boundary conditions. The calculated bending field is $B_B = 1.074$ T. Note that the aspect ratio has been greatly exaggerated, in order to show the directions of the magnetic moments more clearly. All the spins are in the x–y plane.

boundary conditions are used, the multilayer is extensive in the z and x-axes, even though only four strings are actually shown, and (ii) the $N_z = (32)_{YFe_2} + (8)_{DyFe_2}$ is a shorthand notation for the string of 32 monolayers of YFe_2 followed by 8 monolayers of $DyFe_2$.

It is also of interest to see what happens if we move all of the Dy ions into two columns, leaving the other two strings Dy-free. This situation is illustrated in figure 4.

Two principle conclusions can be drawn from a comparison of figures 3 and 4. (1) despite the absence of Dy ions in the two left-hand strings in figure 4, the Fe ions behave as if Dy ions are present. (2) the exchange spring is now determined primarily by the shortened YFe_2 chain below the two Dy-columns. Indeed, the bending field has been increased by some 38.75%, even though the same amount of $DyFe_2$ has been used. The first of these observations can be easily understood. Even though Dy ions are not present, the Y-only strings will mirror those of the Dy-strings (in figure 4) because of the strong Fe–Fe exchange field across the x–y direction. The second observation follows from that of the first. Indeed the calculated bending field of a 2D system with four Dy-strings, all identical to those of the two right-hand columns in figure 4, is $B_B = 1.926$ T, cf $B_B = 1.461$ T, for the four strings shown in figure 4. Moreover, from a comparison of these two bending fields, it is evident that the removal of half the pinning layer only leads to a reduction of 24.1% in the bending field B_B. In general terms, for interface roughness on a small length scale, the bending field is determined primarily by the shortest YFe_2 chain.

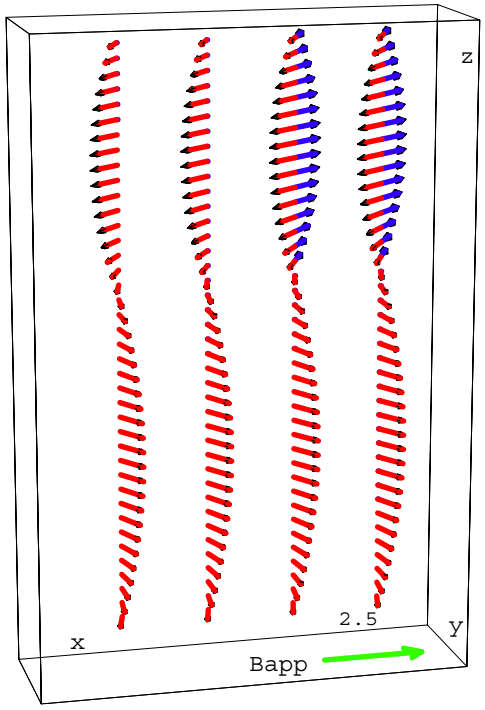

Figure 4. A 2D exchange spring for four strings with $N_{x1} = N_{x2} = 2$ and $N_{z1} = (24)_{YFe_2} + (16)_{DyFe_2}$ and $N_{z2} = (40)_{YFe_2} + (0)_{DyFe_2}$, with cyclic boundary conditions. The calculated bending field is $B_B = 1.461$ T. All the spins are in the x–y plane.

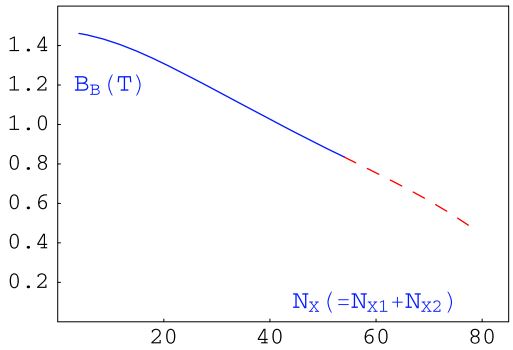

Figure 5. 2D bending field calculations, with cyclic boundary conditions, as a function of $N_x = (N_{x1} + N_{x2})$, for $N_{x1} = N_{x2}$ and $N_{z1} = (24)_{YFe_2} + (16)_{DyFe_2}$ and $N_{z1} = (40)_{YFe_2} + (0)_{DyFe_2}$. The dashed line represents an extrapolation.

Of course if we increase the number of strings, in figure 4 to $N_{x1} = N_{x2} = 6$, 8 etc, at some point the YFe_2 block (N_{x1}) will start to dominate, leading to a decrease in the bending field B_B. This behaviour has been modelled by increasing the period of the patterned structure in the x-direction, $N_{x1} = N_{x2} = 4$, 6, 8, −28 as illustrated in figure 5.

It will be observed that the bending field does indeed fall, as expected. But the fall-off is relatively slow. From the extrapolated results, we find that the bending field falls by ∼1/2 when $N_{x1} = N_{x2} \sim 30$. This corresponds to a total distance N_x of ∼200 Å. We can understand this result as follows. For small N_{x1} the bending field is determined primarily by the shortest YFe_2 string $N = 24$ (see figure 4).

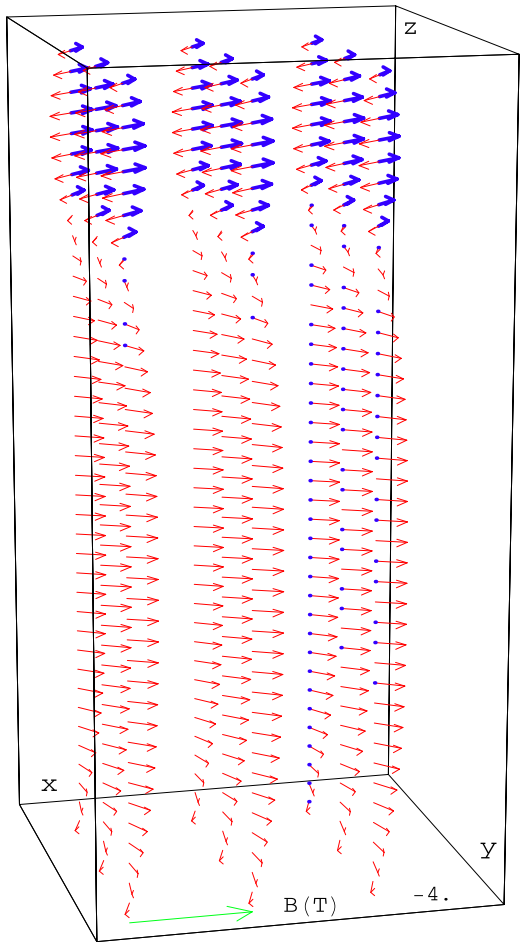

Figure 6. An example of a 3D planar exchange spring in an $N_x = N_y = 3$, $N_z = (32)_{YFe_2} + (8)_{DyFe_2}$ system, with cyclic boundary conditions. The calculated bending field is $B_B = 1.074$ T.

But as N_{x1} is increased, there will come a point when the bending field transition will take place not underneath the $DyFe_2$ strings, but horizontally across the YFe_2 rich areas. Using equation (11), we can make a rough estimate for the bending field to fall by about one-half. We find $N_{x1} \approx 24\sqrt{2} = 34$, in reasonable agreement with figure 5. But, of course, the real situation is more complicated, given the interaction between the springs underneath the $DyFe_2$ layers and those in the YFe_2 rich areas. In such cases, the magnetic exchange spring will be truly 2D in nature, involving angular dispersion in both the x and z-directions.

Finally, when $N_x = 56$ (the right-end of the solid line), the calculation involves a total number of 2240 spins (4480 variables). This roughly represents the present limit of our 2D calculations, using a Mathematica 5 program on a 3.59 GHz computer.

5. 3D magnetic exchange springs

An example of a 3D magnetic exchange spring can be seen in figure 6. The complete loop, showing the expected negative coercivity, is shown in figure 7.

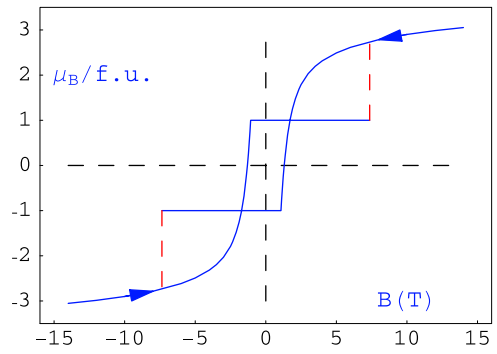

Figure 7. Calculated magnetization loop in 3D for $N_x = N_y = 3$ and $N_z = (32)_{YFe_2} + (8)_{DyFe_2}$, with cyclic boundary conditions. The bending field transition is at 1.074 T.

The magnetization loop in 3D is very similar to that of the 1D model of Bowden *et al* (2003), and Beaujour *et al* (2001). Note the loop exhibits negative coercivity, in that the magnetization goes negative at a finite positive field, as the magnetic spring unwinds.

6. 3D magnetic exchange springs: point defects

Unlike the 1D model, both 2D and 3D calculations can be used to probe the effects of vacancies on magnetic exchange springs. An example can be seen in figure 8. Here an iron vacancy has been placed in the middle of one of the YFe_2 springs. The bending field in this case is $B_B = 1.080$ T, an increase of some 0.6% on the defect-free system. However, if the vacancy is placed at the top of one of the YFe_2 chains, the bending field is decreased by 1.3%. We can understand these two results, qualitatively, as follows. If an iron moment is removed from the centre of the chain, the Zeeman interaction which drives the exchange spring is reduced. This leads to an increase in B_B because a larger applied field is required to drive the transition. However, when the vacancy is placed at the top of the YFe_2 chain, the pinning of the spring is reduced at that point, leading to a decrease in B_B. More results for 1–3 vacancies can be seen in table 1. Note that in the main the effect of Fe vacancies is small, a few per cent. Given that each Fe ion is surrounded by six neighbours, it is evident that the loss of $\sim 1/6$ exchange field at one or more sites, does not unduly affect the majority of the Fe spins.

In table 1, we have also listed the effects due to inserting Dy ions into the middle of the YFe_2 strings. Here the changes in the bending field are much more significant than those caused by Fe vacancies. For example if a monolayer of 9 $DyFe_2$ moments is taken from the bottom of the $DyFe_2$ strings (layer $z = 33$) and placed in the middle of the YFe_2 string (layer $z = 17$), the change in the bending field amounts to +57.6%. Note that this increase has been achieved without changing the overall number of $DyFe_2$ and YFe_2 layers. This substantial increase can be understood as follows. The Dy ions stiffen the YFe_2 exchange springs in two ways: (i) via the Dy-anisotropy, which favours the x-axis, and (ii) via the Dy–Zeeman interaction, which acts against the formation of the magnetic exchange spring. The way is open therefore, to modify the properties of magnetic exchange springs, by inserting differing RE ions into the middle of the YFe_2 strings.

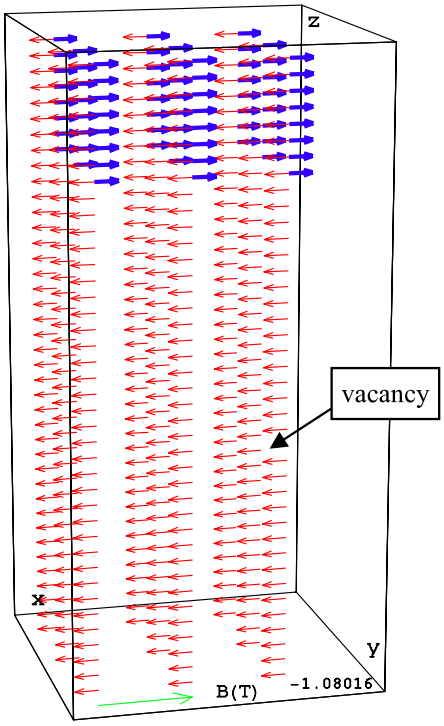

Figure 8. An Fe vacancy at **r**(1,3,16) i.e. half-way up the YFe_2 spring. The calculated bending field is $B_B = 1.080$ T, an increase of +0.400% over the defect-free system.

Table 1. Changes in the bending field B_B brought about by various point defects, in a 3D planar exchange spring, for a nominal $N_{YFe_2}/N_{DyFe_2} = 32/8$ and $K_{anis} = -10$. The vacancies 1–3 are along a cube edge in the x-direction.

Defect-type	No.	Bending field (T)	$\Delta B_B/B_B$ (%)
None	0	1.073 939	0
Mid-spring Fe vacancy	1	1.080 163	0.622
Mid-spring Fe vacancy	2	1.086 441	1.250
Mid-spring Fe vacancy	3	1.092 768	1.883
Top-spring Fe vacancy	1	1.060 9355	−1.300
Top-spring Fe vacancy	2	1.044 0353	−2.990
Top-spring Fe vacancy	3	1.021 344	−5.259
Mid-spring Dy ion	1	1.142 9098	6.897
Mid-spring Dy ion	2	1.211 1585	13.722
Mid-spring Dy ion	3	1.278389	20.445
Mid-spring Dy ion	9	1.649 718	57.578
Mid-spring Dy ion	18	2.098 697	102.476

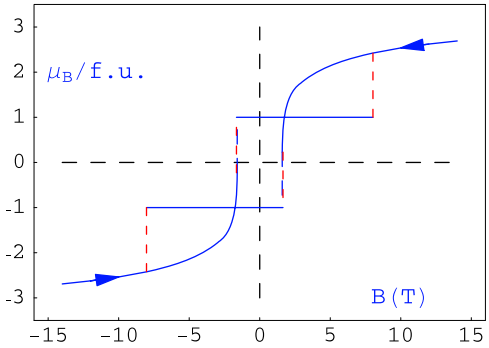

Figure 9. Calculated magnetization loop in 3D for a nominal $N_{YFe_2}/N_{DyFe_2} = 8/32$, with $N_x = N_y = 3$ and $N_z = (16)_{YFe_2} + (1)_{DyFe_2} + (16)_{YFe_2} + (7)_{DyFe_2}$ i.e. one plane of $DyFe_2$ atoms removed from the bottom of the $DyFe_2$ strings and placed into the middle of the YFe_2 strings ($z = 17$). Note that the 'bending field' B_B is now discontinuous (dotted lines).

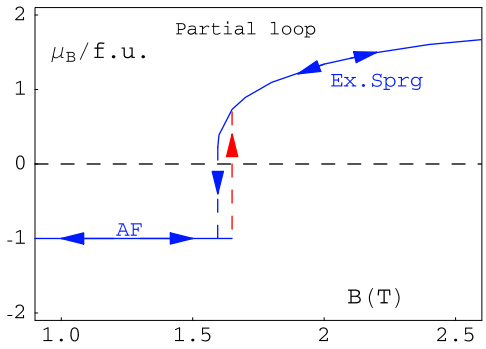

Figure 10. A partial loop. The 'bending field' B_B is discontinuous (dotted lines) and hysteretic: 1.650 T on the way up and 1.595 T on the way down.

Finally, in figure 9 we show the calculated magnetic loop for one $DyFe_2$ layer placed into the middle of the YFe_2 strings. From a comparison of figures 7 and 9, it will be seen that the bending field B_B is increased, while the saturation moment is slightly reduced. But more importantly, the 'bending field transition' is now discontinuous and hysteretic. This is due primarily to the anisotropy of the mid-spring Dy ions. As the exchange spring unwinds, the mid-spring $DyFe_2$ layer is forced by the YFe_2-spring to point along a hard axis. As a result, the Dy ions act so as to pin the magnetic exchange spring. But, as the magnetic field is reduced below a critical value, the Dy ions over-reach the hard 90° direction, leading to a sudden magnetic collapse of the spring to the AF-state. This is illustrated more clearly in figure 10, which shows a partial loop around the 'bending field transition'.

7. Conclusions

In this paper, 1D models of magnetic exchange springs have been extended to 2D and 3D. In practice, the 2D and 3D models represent an improvement on the 1D model, because they allow effects due either to defects and/or deliberate doping to be investigated.

2D calculations have been presented, which show that the properties of domain walls can be significantly altered by modifying the structural configuration of the hard/soft interface. Such calculations have relevance in the study of both interface roughness and patterned materials. In general, for relatively small interface roughness in the lateral (x) dimension, the bending field is determined primarily by the smallest of the YFe_2 strings.

3D calculations have also revealed novel exchange spring behaviour. In particular, we have probed the effect of defects on the properties of magnetic exchange springs, in the $DyFe_2/YFe_2$ system. It was found that point defects such as Fe vacancies have little effect on the bending field transition, in marked contrast to the 1D model. However, when RE ions are placed in the centre of the soft YFe_2 springs, significant changes can be brought about in the properties of magnetic exchange springs.

Finally, a new phenomenon has been postulated: *magnetic-exchange spring collapse*. In the past, exchange springs have been considered reversible. However, when selected RE ions are placed into the middle of a soft exchange spring, the bending field transition can become discontinuous and irreversible.

Acknowledgment

The authors gratefully acknowledge support from the Engineering and Physical Sciences Research Council.

References

Amato M, Pini M G and Rettori A 1999 *Phys. Rev.* B **60** 3414
Amato M, Rettori A and Pini M G 2000 *Physica* B **275** 120–3
Armitage J G M, Dumelow T, Riedi P C and Abell J S 1989 *J. Phys.: Condens. Matter* **1** 3987–94
Beaujour J-M L, Bowden G J, Gordeev S, de Groot P A J, Rainford B D, Ward R C C and Wells M R 2001 *Appl. Phys. Lett.* **78** 964
Bowden G J, Beaujour J-M L, Goordeev S, de Groot P A J, Rainford B D and Sawicki M 2000 *J. Phys.: Condens. Matter* **12** 9335–46
Bowden G J, Beaujour J-M L, Zhukov A A, Rainford B D, de Groot P A J, Ward R C C and Wells M R 2003 *J. Appl. Phys.* **93** 6480
Buschow K H J 1977 *Rep. Prog. Phys.* **40** 1179–256
Coey J M D and Skomski R 1993 *Phys. Scr.* T **49** 315
Dumesnil K, Dutheil M, Dufour C and Mangin Ph 2000 *Phys. Rev.* B **62** 1136
Fitzsimmons M R, Park S, Dumesnil K, Dufour C, Pynn R, Borchers J A, Rhyne J J and Mangin Ph 2006 *Phys. Rev.* B **73** 134413
Fullerton E E, Jiang J S and Bader S D 1999 *J. Magn. Magn. Mater.* **200** 392
Fullerton E E, Jiang J S, Grimsditch M, Sowers C H and Bader S D 1998 *Phys. Rev.* B **58** 12193
Gordeev S, Beaujour J-M L, Bowden G J, de Groot P A J, Rainford B D, Ward R C C, Wells M R and Jansen A G M 2001 *Phys. Rev. Lett.* **87** 186808
Goto E, Hayashi N, Miyashita T and Nakagawa K 1965 *J. Appl. Phys.* **36** 2951–8
Jiang J S, Pearson J E, Liu Z Y, Kabius B, Trasobares S, Miller D J, Bader S D, Lee D R, Haskel D, Srajer G and Liu J P 2004 *Appl. Phys. Lett.* **85** 5293
Kneller E F 1991 *IEEE Trans. Magn.* **70** 3588

Sawicki M, Bowden G J, de Groot P A J, Rainford B R, Beaujour J-M L, Ward R C C and Wells M R 2000 *Phys. Rev.* B **62** 5817–20

Trallori L, Pini M G, Retorri A, Maccio M and Politi P 1996 *Int. J. Mod. Phys.* B **10** 1935

Trallori L, Politi P, Retorri A, Pini M G and Villain J 1994 *Phys. Rev. Lett.* **72** 1925

Ulrich J, Maat S, Lee R J and Fullerton E E 2004 *IEEE Trans. Magn.* **40** 2537

Zimmermann J P, Bordignon G, Boardman R P, Fischbacker T, Fangohr H, Marin K N, Bowden G J, Zhukov A and de Groot P A J 2006 *J. Appl. Phys.* **99** 08B904